Electronic Supplementary Material (ESI) for Journal of Materials Chemistry A.
This journal is © The Royal Society of Chemistry 2019

Supporting Information

Vertically constructed monolithic electrodes for sodium ion batteries: toward low tortuosity and high energy density

Ping Li,[a,b] Yanan Wang,[c] Jong Yeob Jeong,[b] Xiaoming Gao,[c] Kan Zhang,*[a] Anne Neville,[d] Shusheng Xu*[d] and Jong Hyeok Park*[b]

[a] MIIT Key Laboratory of Advanced Display Materials and Devices, Institute of Optoelectronics and Nanomaterials, School of Materials Science and Engineering, Nanjing University of Science and Technology, Nanjing 210094, People's Republic of China

[b] Department of Chemical and Biomolecular Engineering, Yonsei University, 50 Yonsei-ro, Seodaemun-gu, Seoul 120-749, Republic of Korea

[c] State Key Laboratory of Solid Lubrication, Lanzhou Institute of Chemical Physics, Chinese Academy of Sciences, Lanzhou 730000, People's Republic of China

[d] Institute of Functional Surfaces, School of Mechanical Engineering, University of Leeds, Leeds, LS2 9JT, UK

Corresponding Author:

Email: zhangkan@njust.edu.cn
Email: S.Xu1@leeds.ac.uk
Email: lutts@yonsei.ac.kr

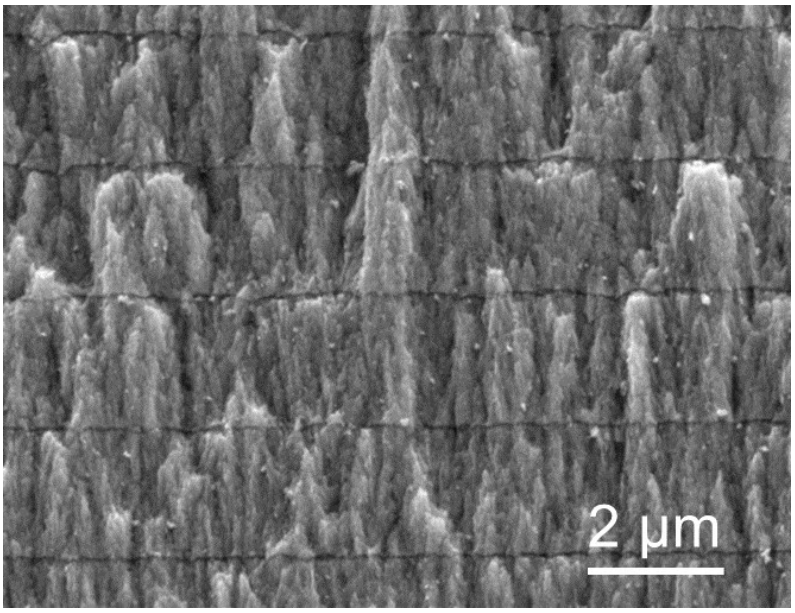

Fig. S1 SEM image of the cross-section of the WS_2/C monolithic electrode after prolonging the carbon deposition time to clearly show the introduced carbon layers.

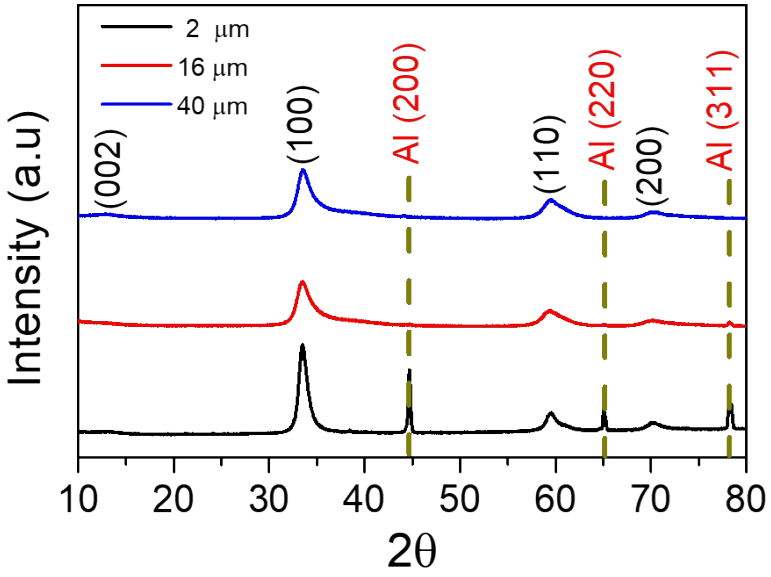

Fig. S2 XRD patterns of PVD-deposited monolithic electrodes with different thicknesses from 2 μm to 40 μm.

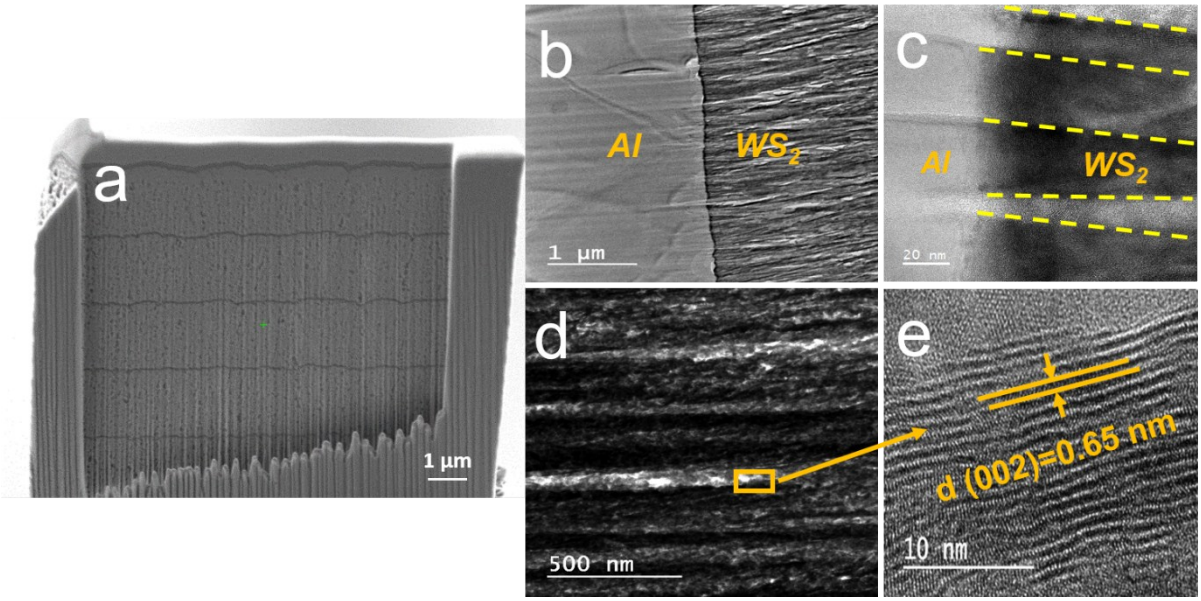

Fig. S3 (a) SEM image of the as-prepared FIB sample from the cross-section of the WS_2/C monolithic electrode. (b, c) TEM images of the interface of the WS_2 arrays and Al foil. (d, e) TEM and HRTEM images of part of the WS_2 arrays.

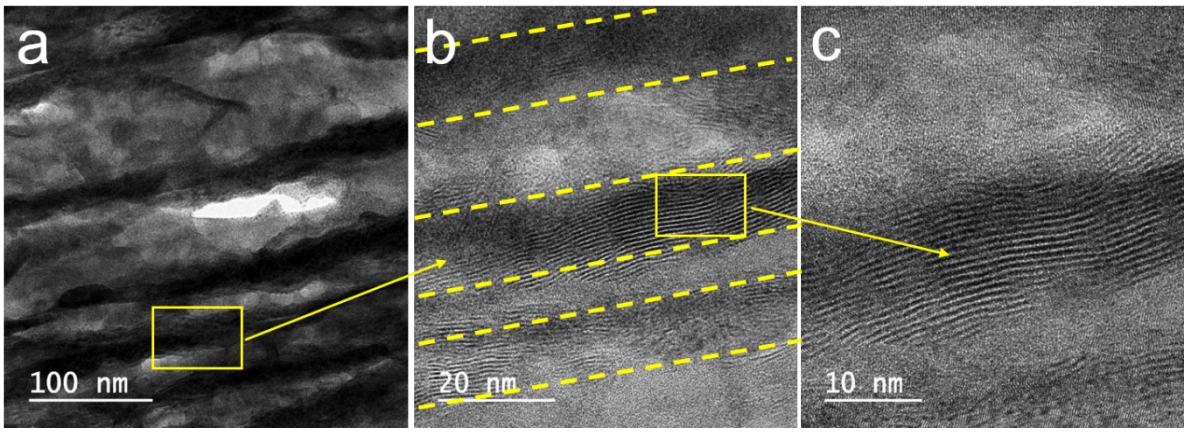

Fig. S4 (a, b, c) Gradually enlarged TEM images of the WS_2 arrays section that showed the vertically oriented van der Waals gaps of WS_2.

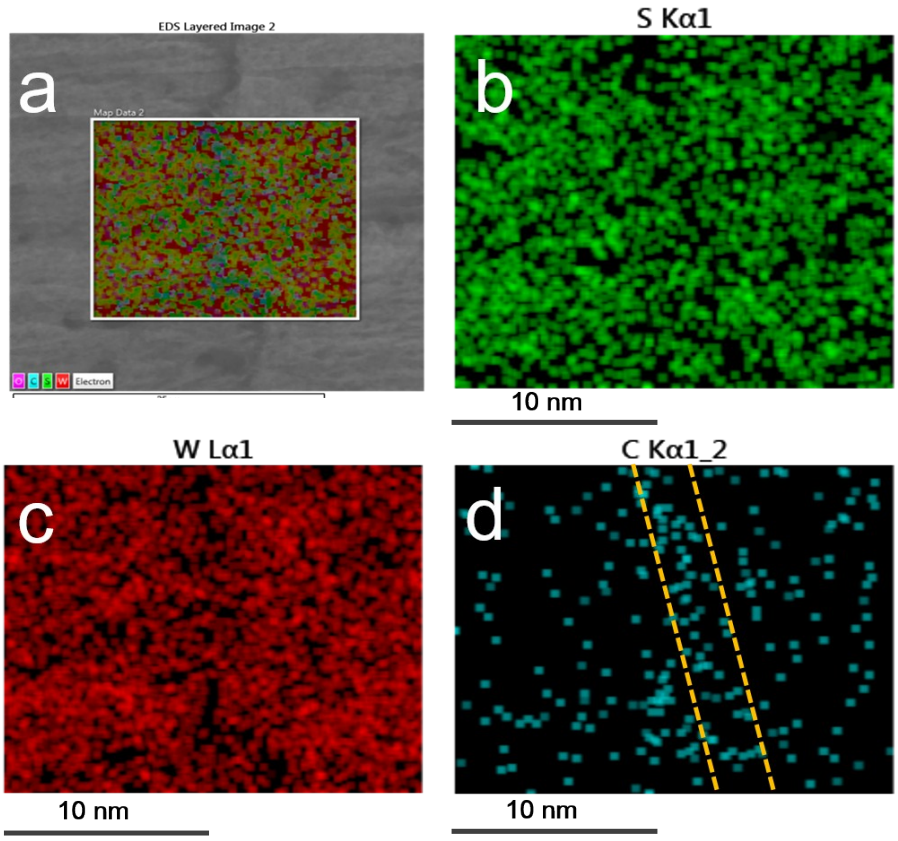

Fig. S5 (a-d) Element mapping of the partition between the WS_2 arrays and introduced C agents.

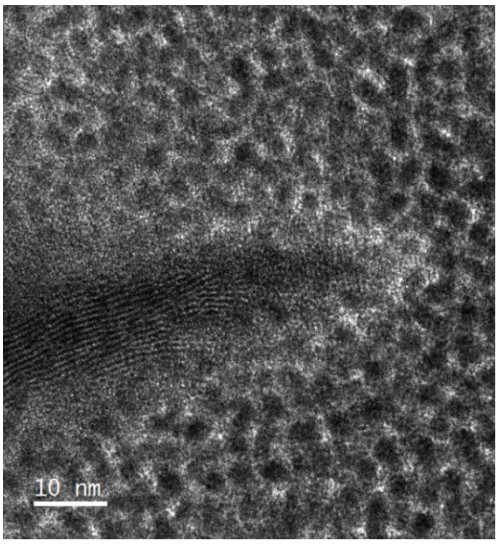

Fig. S6 Enlarged TEM images showing the introduced carbon agents located on the terminus of the WS_2 arrays as dots.

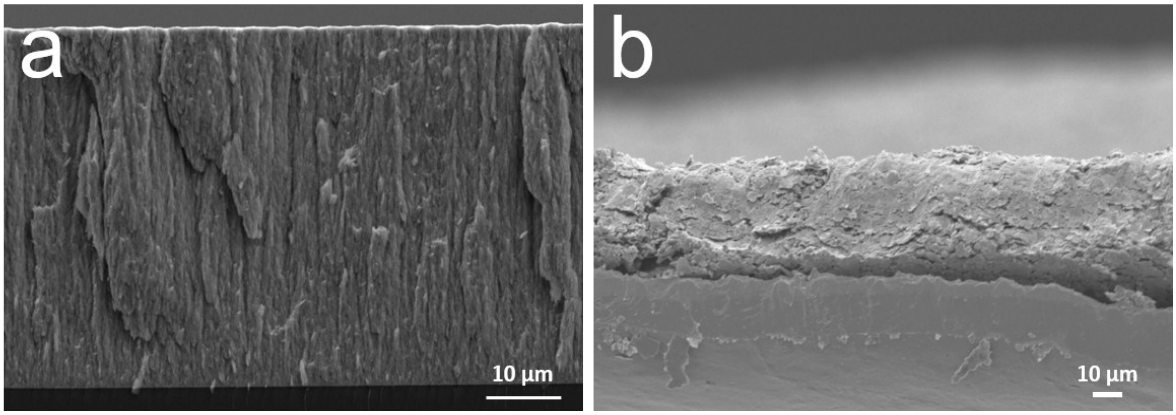

Fig. S7 SEM images of the cross-sections of (a) a PVD-deposited pure WS_2 monolithic electrode with a thickness of 40 µm and (b) a slurry paste WS_2 powder electrode with a thickness of 40 µm.

Table S1. Redox peaks of the pasted electrode and the vertical deposited electrode (red marked peaks represent the conversion reaction).

	Cathodic peak (V)	**Anodic peak (V)**
Pasted electrode	2.02, 1.38, 1.09, 0.91, 0.58	0.38, 0.75, 0.89, 1.37, 1.86, 2.26, 2.58
Vertical electrode	1.95, 0.89, 0.58	0.38, 0.75, 0.89, 1.34, 1.76, 2.24, 2.76

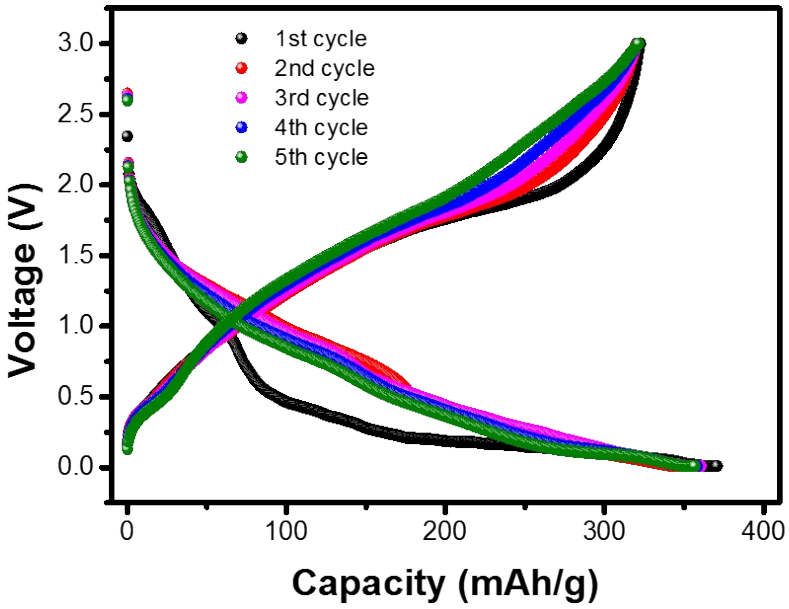

Fig. S8 Galvanostatic charge and discharge profile of the PVD-deposited WS_2/C monolithic electrode.

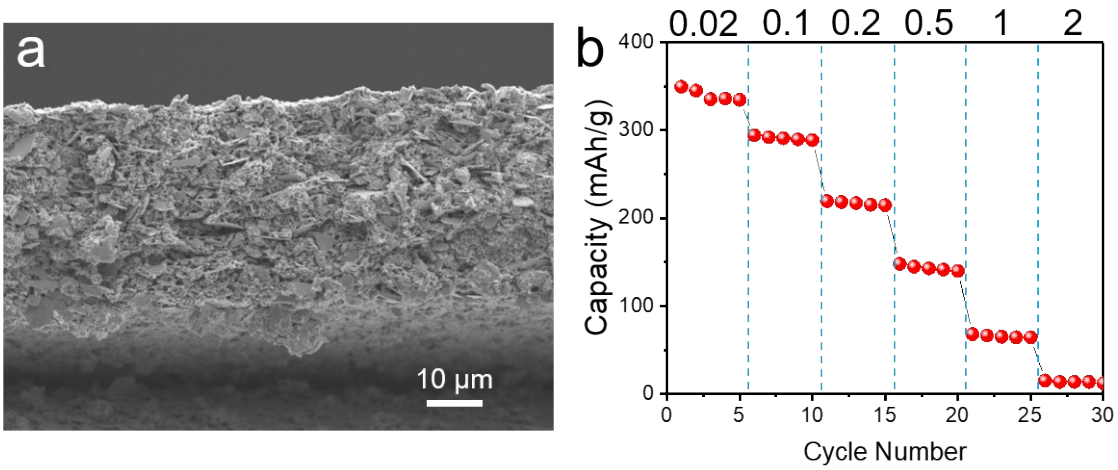

Fig. S9 (a) The cross-section SEM image and (b) C-rate performance of a slurry pasted randomly-aligned WS_2 nanosheet electrode.

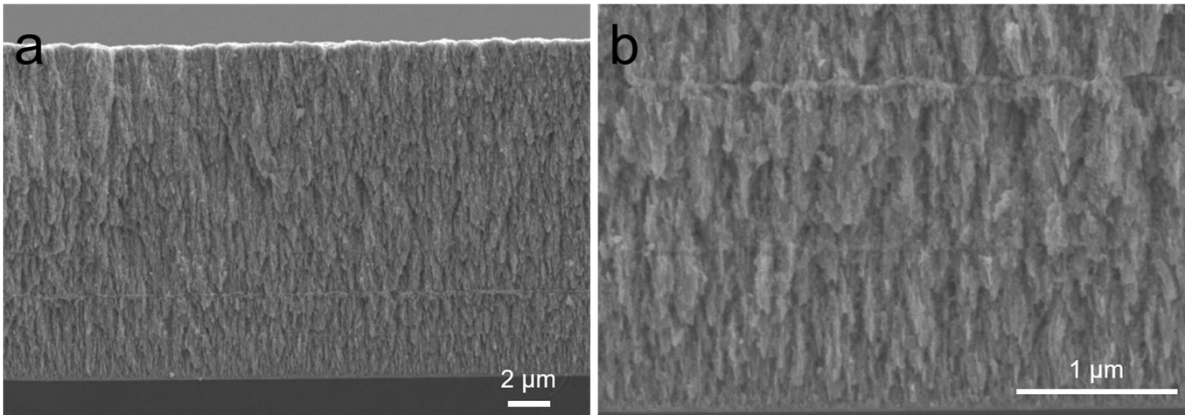

Fig. S10 (a, b) SEM images of the cross-sectional view of the 16 μm thick WS_2/C monolithic electrode.

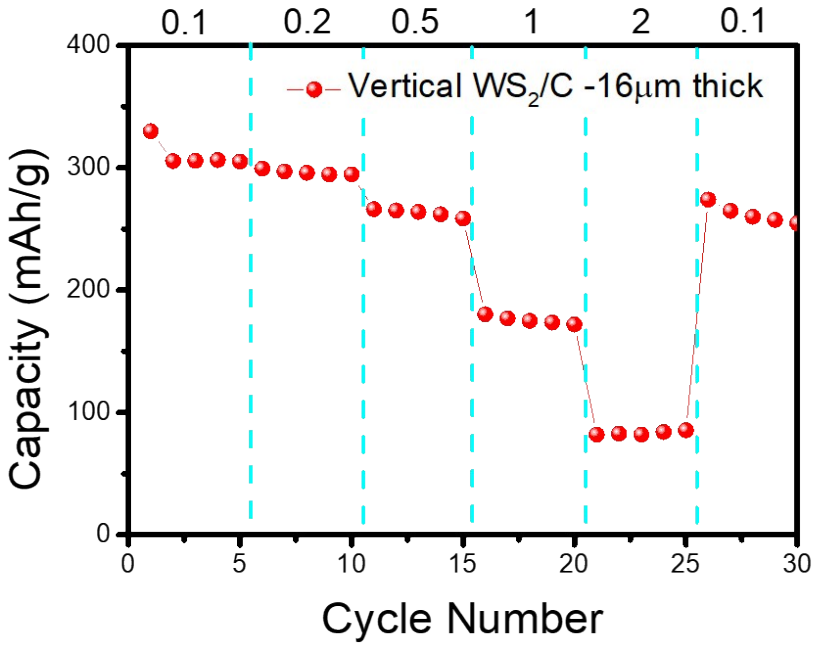

Fig. S11 Rate performance of the 16 μm WS_2/C monolithic electrode at different current densities.

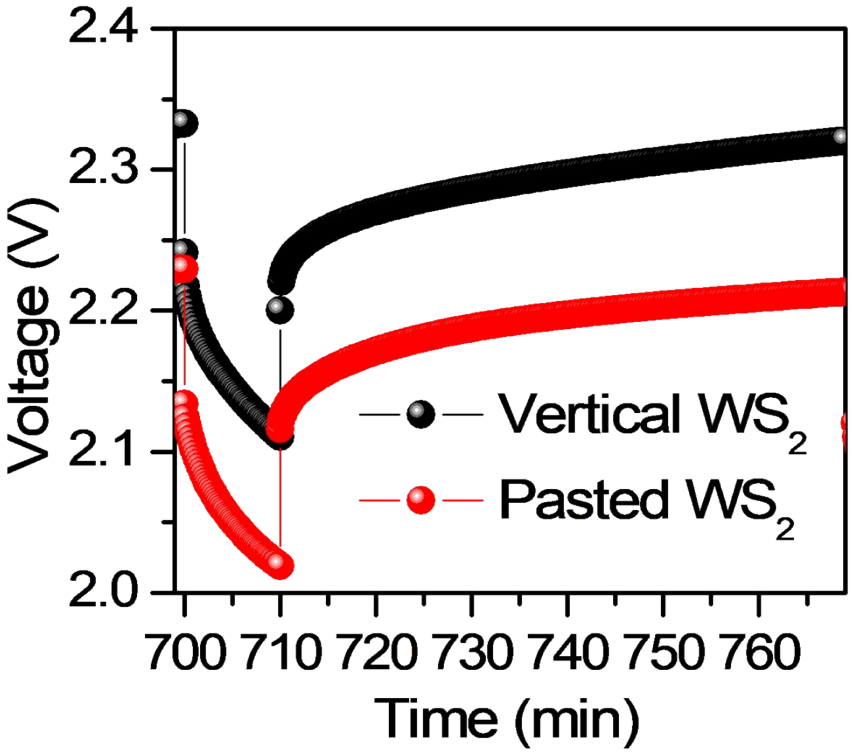

Fig. S12 Calculation of the Na-ion diffusivity of the pure WS_2 monolithic electrode and traditional slurry paste WS_2 powder electrode based on GITT.

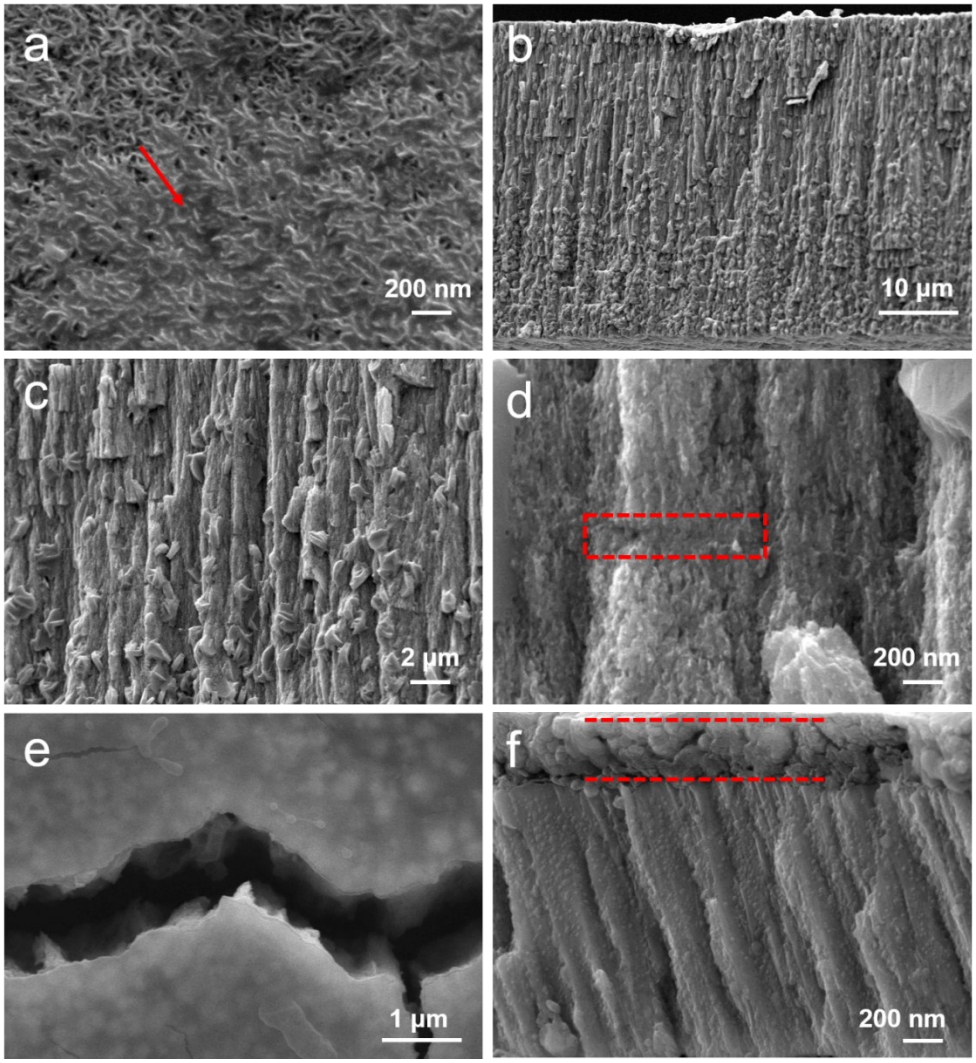

Fig. S13. SEM images of the vertical WS_2/C electrode after cycles. (a) top view of the electrode after one cycle time, the red arrow points the SEI layer region. (b, c, d) cross-view of the electrode after one cycle time, the red dashed box shows the introduced carbon. (e) top view of the electrode after 100 cycle time. (f) cross-view of the electrode after 100 cycle time, the region between the two red dashed line is SEI layer on the top of the electrode.

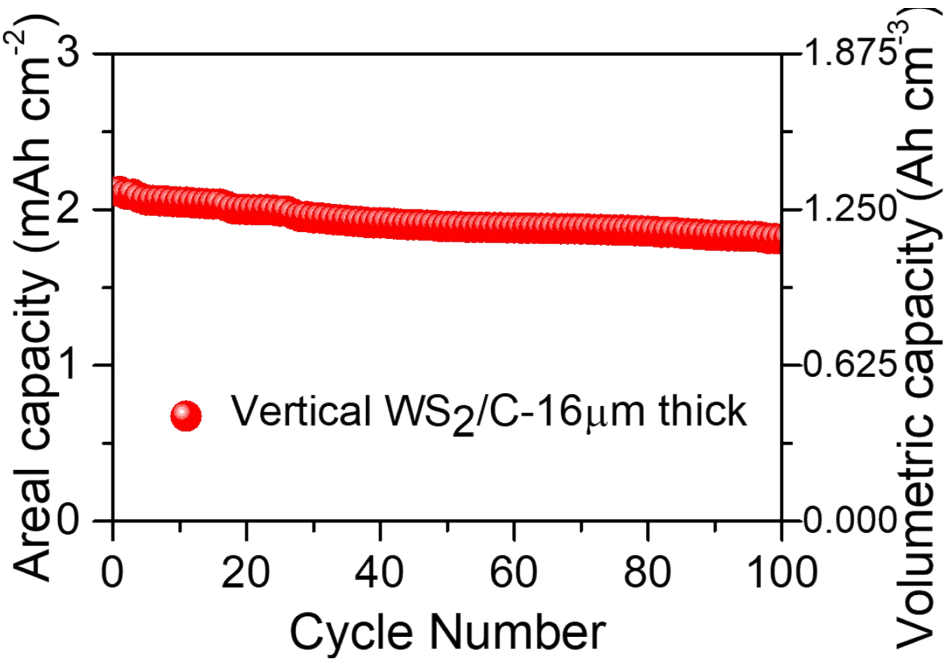

Fig. S14. Areal capacity and volumetric capacity of the 16 μm WS_2/C monolithic electrode.

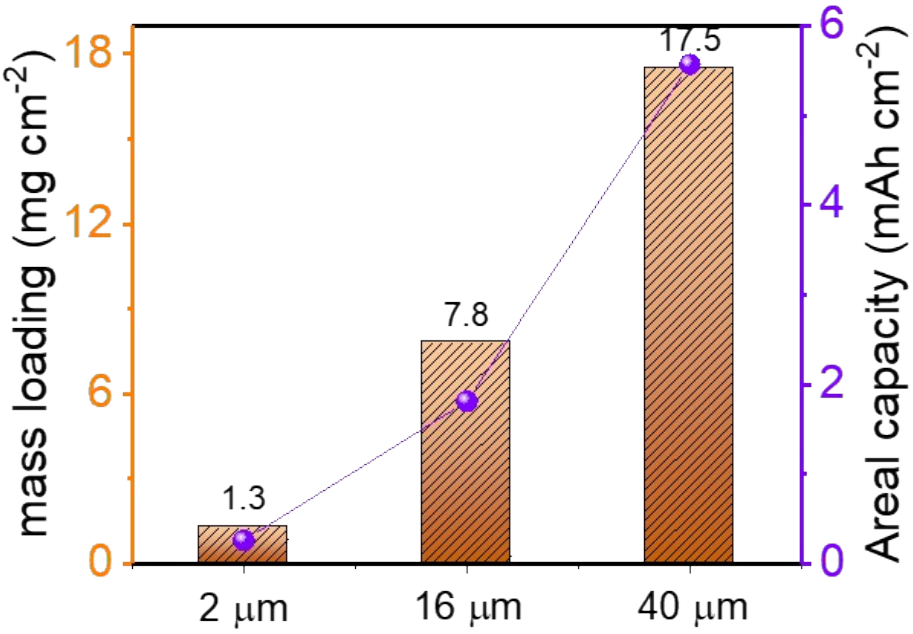

Fig. S15. The relationship between the areal capacity, mass loading, and thickness of the WS_2/C monolithic electrode.

Table S2. Comparison of our work and other reports with other strategies to achieve high-energy-density SIBs.

	Materials	Mass Loading (mg cm^{-2})	Areal Capacity (mAh cm^{-2})	Volume Capacity (Ah cm^{-3})	Current Density (mA g^{-1}, mA cm^{-2})	Thickness (μm)
Our Work	WS_2/C	17.5	5.57	1.39	100 mA g^{-1}	40
2016 ACS Nano	MoS_2/SWNT	15	>6.0	~0.65	0.2 mA cm^{-2}	100
2016 AEM	Mesoporous wood carbon	55	13.16	0.16	0.55 mA cm^{-2}	850
2016 ACS Nano	Self-branched 2D SnS_2	3.98	3.7		0.8 mA cm^{-2}	
2017 Materials Research Bulletin	SnO_2 nanospheres	7.8	3.492	0.97	20 mA g^{-1}	36
2017 AEM	Amorphous MoS_3	12	>6.0	~1	100 mA g^{-1}	65
2017 JMCA	$Ni_3V_2O_8$/carbon cloth	4	2.6		500 mA g^{-1}	
2018 Nano Energy	CaV_4O_9 microflowers	3.65	1	0.19	100 mA g^{-1}	53.8
2018 Nanoscale	FeSe@FeS	8	2.8		500 mA g^{-1}	